Available online at www.eccomasproceedia.org
Eccomas Proceedia COMPDYN (2025) 4 70-4 86

ECCOMAS
Proceedia

COMPDYN 2025
10th ECCOMAS Thematic Conference on
Computational Methods in Structural Dynamics and Earthquake Engineering
M. Papadrakakis, M. Fragiadakis (eds.)
Rhodes Island, Greece, 15-18 June 2025

BEYOND SPECTRAL ACCELERATION: ENHANCING SEISMIC RESPONSE PREDICTION IN BRIDGES WITH NEXT-GENERATION INTENSITY MEASURES

Savvinos Aristeidou[1], **Gerard J. O'Reilly**[1]

[1]Centre for Training and Research on Reduction of Seismic Risk (ROSE Centre)
Scuola Universitaria Superiore IUSS Pavia
Palazzo del Broletto, Piazza della Vittoria 15, Pavia 27100, Italia
e-mail: {savvinos.aristeidou,gerard.oreilly}@iusspavia.it

Abstract. *There exists extensive literature evaluating intensity measures (IMs) on criteria such as sufficiency, efficiency, and bias, but most of these studies primarily concentrate on the conditioning IM while neglecting the effect of matching the conditional distributions of other IMs. This study aims to identify the optimal combination of conditioning and matching IMs to improve predictive accuracy in structural response estimates while more comprehensively representing seismic hazard characteristics across varying intensity levels. Leveraging a recent generalised ground motion model (GGMM) and associated correlation models, this work explores both next-generation and conventional IMs — including spectral acceleration, Sa, average spectral acceleration, Sa_{avg}, filtered incremental velocity, $FIV3$, and significant duration, Ds_{575} — each of which captures distinct characteristics of ground motion. Specifically, Sa captures spectral amplitude, Sa_{avg} provides insights into spectral amplitude and shape, $FIV3$ conveys information on consecutive velocity pulses which are critical for collapse risk, and Ds_{575} characterizes significant duration, informing on the energy contained in ground motion. We conducted comparative multiple stripe analyses (MSA) on seven case study bridges. The bridges are represent typical European design, with reinforced concrete (RC) piers and continuous deck. Realistic cyclic and in-cycle strength and stiffness degradation is incorporated in the numerical model. Probabilistic seismic hazard analysis (PSHA) was performed for all the conditioning IMs for a site in Erzincan, Turkey. We evaluated eleven different ground motion selection strategies, with varying levels of hazard-consistency. Notably, results indicate that when matching the Sa spectrum alone, the theoretical distributions of $Sa_{avg}(T_1)$ and $FIV3(T_1)$ are also matched, without additional consideration. Additionally, matching the theoretical generalized conditional IM (GCIM) distributions of 'secondary' IMs yielded lower response medians and dispersions. Conditioning on different IMs was shown to impact the performance depending on the intensity level. This study's primary contribution lies in demonstrating how next-generation IMs can enhance seismic risk assessment accuracy for structures by providing a more nuanced representation of seismic hazard.*

Keywords: Bridges, risk assessment, generalised conditional intensity measure, intensity measures, probabilistic seismic hazard analysis, hazard consistency.

ISSN:2623-3347
Peer-review under responsibility of the organizing committee of COMPDYN 2025.
doi: 10.7712/120125.12742.25 04

1 INTRODUCTION

Seismic risk assessment of structures, particularly bridges, has evolved significantly over the years with advancements in structural numerical modelling, probabilistic seismic hazard analysis (PSHA) models, and ground motion input characterisation. Traditional approaches often relied on simpler conditioning intensity measures (IMs), such as peak ground acceleration, PGA, which, while convenient, is insufficient in capturing the complex response of multi-modal and multi-component systems like bridges [1, 2]. Recent research has highlighted the importance of utilising advanced IMs, that better reflect the underlying seismic hazard characteristics, which can be of higher engineering interest (e.g., [3, 4]). These advanced (or next-generation, as dubbed here) IMs not only improve the accuracy of seismic hazard representation but also enhance the reliability of risk predictions. Building on this foundation, some IMs of engineering interest were integrated herein with advanced ground motion selection methods to assess the level to which they enhance seismic risk for bridge structures.

This study leverages recently developed generalised ground motion model (GGMM) and correlation models [5, 6]. These models enabled improved predictive power and more accurate representation of seismic hazard, since they estimate a wide range of IMs. The practical applicability of the aforementioned models in ground motion record selection and risk assessment is also demonstrated.

A review of the evolution of ground motion record selection for structures, with a particular focus on bridges, is given in the following, positioning this work within the context of state-of-the-art in the field. Next, the case study bridge structures and their numerical models are described. Ground motion selection strategies and seismic hazard analysis of the conditioning IMs are then introduced, setting the stage for the subsequent multiple stripe analysis (MSA). Finally, the chapter concludes with a comparison and critical evaluation of the structural response estimations, highlighting the significance and practical implications of the findings.

2 GROUND MOTION INPUT FOR BRIDGE STRUCTURES

The selection and scaling of ground motion input are critical steps in the seismic analysis of bridge structures. Ground motions are typically selected and scaled based on seismic scenarios that match the site-specific hazard, coming from either PSHA, or design code requirements. Scaling is usually done to achieve a specific value of the conditioning IM, and subsequent selection to match the spectral shape (or distribution in the probabilistic case). Many studies continue to rely on IM definitions, such as PGA or spectral acceleration, Sa, at a fixed period [7, 8, 9] for regional risk assessments. Although they recognise that these are not ideal, they are often used as a baseline standard due to their simplicity and widespread adoption for convenience.

There are several ground motion selection approaches listed and briefly described in the following. The uniform hazard spectrum (UHS)-based approach, commonly employed in seismic design codes such as Eurocode 8 [10] and ASCE 7 [11], involves selecting and scaling ground motions to match the UHS for a given return period. However, the UHS does not really represent the physical characteristics of individual earthquakes, but instead aggregates the seismic hazard across all potential magnitudes, distances, and fault mechanisms, selecting the maximum intensity at each oscillation period for a given return period. This tends to overestimate hazard at certain periods and lead to conservative design requirements. While UHS-based selection remains prevalent due to its simplicity and alignment with design code requirements, advanced methods such as the conditional spectrum (CS) [12] and generalised conditional intensity measure (GCIM) [13] offer a more rigorous probabilistic framework, with a more nuanced repre-

sentation of ground motion variability. They offer the capability of conditioning the selection process on a specific IM or multiple IMs. These methods ensure consistency with PSHA and are particularly suited for performance-based assessments. Scenario-based assessment [14], on the contrary, selects ground motions that represent specific seismic events, such as characteristic earthquakes from a known nearby fault. While this approach provides realistic inputs for scenario-specific studies, which can sometimes be easier to communicate, it lacks the versatility required for probabilistic risk evaluations.

This study primarily investigates the CS and GCIM approaches, along with just scaling ground motions to a target $Sa(T_1)$ level.

3 CASE STUDY STRUCTURES

3.1 General description

To examine the influence of the different combinations of conditioning and matching the different IMs on the seismic assessment of bridges, seven multi-span bridges, each comprising either of 4 or 8 spans of 50 m, were analysed. These bridges, previously studied by Pinho et al. [15] and O'Reilly [16] are representative of typical European bridge designs, featuring reinforced concrete (RC) piers designed according to Eurocode 8 [10]. The piers have a hollow rectangular cross-section, while the deck is continuous, with reinforcement details depicted in Figure 1. Pier heights are either 7 m, 14 m, or 21 m, and the bridges were categorised as regular or irregular based on the pier height configurations along their length. Table 1 summarises the modal properties of the bridge structures in the transverse direction, and their classification as either regular or irregular, with additional illustrations shown in Figure 2.

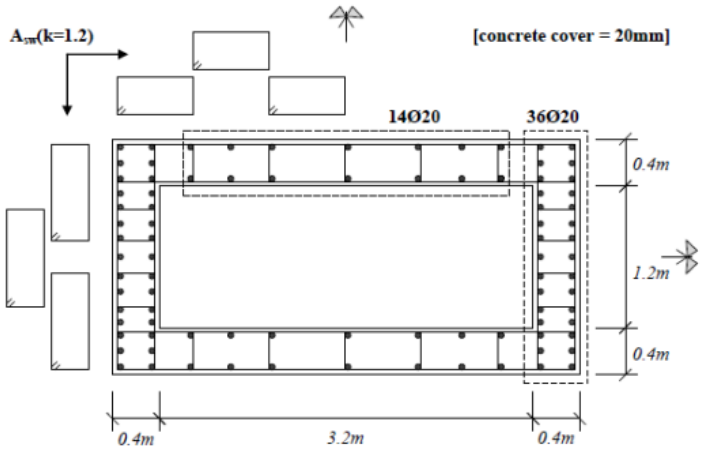

Figure 1: Illustration of structural detailing of the pier cross section [15]. The shorter side of the section is placed in the direction of the bridge deck

The longitudinal reinforcement is consisted of 20 mm diameter bars evenly spaced at 110 mm along the shorter dimension, 310 mm along the longer dimension, and 600 mm for the innermost bars. The concrete cover thickness is 20 mm, with reinforcement yielding at 500 MPa and a concrete compressive strength of 42 MPa. By considering bridges with varying span number and pier height arrangement, and consequently different stiffness distributions, the study aimed to (1) evaluate the effects of period elongation resulting from damage to the pier elements, (2) explore the relevance of regularity/irregularity of the bridge, (3) investigate the influence of multiple significant response modes of bridge structures, and (4) achieve a level

Table 1: Modal properties of each case study bridge structure

ID	Type	T_1 [s]	T_2 [s]	T_3 [s]	$\%M_1$	$\%M_2$	$\%M_3$	$\Sigma\%M$
B-1	Irregular	0.555	0.447	0.277	30	8	27	65
B-2	Irregular	0.555	0.474	0.253	30	19	5	53
B-3	Regular	0.483	0.475	0.223	32	0	66	98
B-4	Regular	0.508	0.475	0.307	6	0	77	94
B-5	Regular	0.479	0.479	0.225	16	0	76	92
B-6	Irregular	0.494	0.474	0.360	3	10	29	42
B-7	Irregular	0.556	0.436	0.387	11	7	35	53

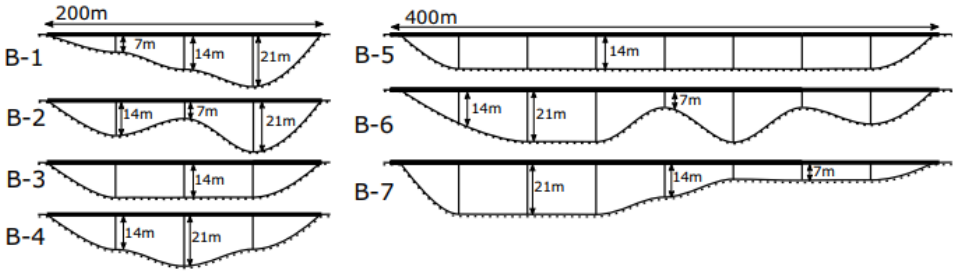

Figure 2: Illustration of the longitudinal profile of the case study bridge structures. Adapted from O'Reilly [16]

of generalisation for different structural configurations of bridge structures.

3.2 Numerical modelling and EDP definition

A numerical model for each bridge was adapted to OpenSeesPy [17] from the existing OpenSees model detailed in O'Reilly and Monteiro [18]. The deck system was modelled as a continuous elastic beam-column element with effective cross-sectional properties and distributed mass. As noted by Pinho et al. [15], the piers were modelled as fixed at their bases and rigidly connected to the underside of the deck, while the deck ends rest on linear pot bearings at the abutments. Although a more refined foundation model could have been implemented, it was deemed unnecessary for the focus of this study, which focusses on the relative comparison of different ground motion selection strategies.

The pier elements were represented using lumped plasticity models, with their parameters derived from moment–curvature analysis of the corresponding fibre-based section. To capture the rupture of the reinforcement bars and the subsequent loss of strength in the pier sections, the *MinMax* criterion was applied in OpenSeesPy, which simulated the loss of strength in the rebars when a predefined strain threshold was exceeded. This rupture strain was set at 0.10, based on Priestley et al. [19] for reinforcement steel in European bridges. The only difference from the modelling parameters described in O'Reilly and Monteiro [18] and O'Reilly [16] is the use of the *HystereticSM* material for the lumped plasticity hinges. This material was implemented with a pinching factor for deformation during reloading of 0.8, a pinching factor for force during reloading of 0.2, a damage parameter due to ductility of 0.001, and a damage parameter due to energy of 0.0001. Incorporating cyclic and in-cycle stiffness and strength degradation was essential here for two main reasons: firstly, to capture the effects of matching (or not) the theoretical GCIM distribution of significant duration, Ds, and the implications of matching and/or conditioning to filtered incremental velocity, $FIV3$; and secondly, to ensure the model exhibits behaviour that more closely approximates real-world structural response.

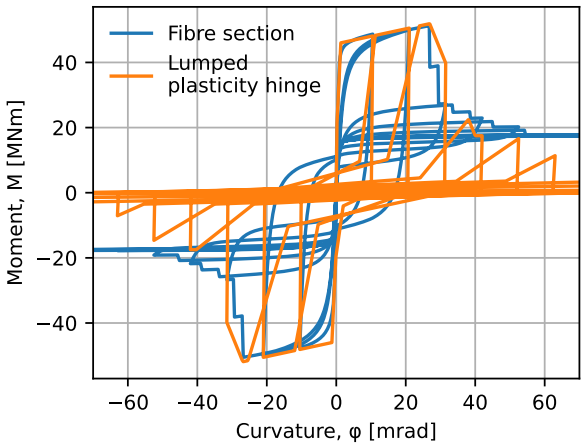

Figure 3: Moment curvature analysis of bottom section of the Pier with 7 m height. 10 cycles of unloading/reloading are shown here as an example, with equal curvature increments until the target curvature

To characterise the structural response under increasing intensity, an appropriate engineering demand parameter (EDP) was required. In bridges, the absence of a dominant mode or a clearly critical element complicates the selection of a suitable EDP. While global EDP, such as peak deck displacement, can be employed, they may fail to adequately capture the extent of damage in piers with varying heights. Given the structural configuration of the bridges, the piers were identified as the critical elements susceptible to structural damage. Since piers were fixed at their base and rigidly connected to the deck, the largest inelastic demand occurs at their base.

Considering the simplicity of the bridge models used in this study, element-specific EDPs were preferred. Specifically, the peak transient section curvature at the base of the piers was monitored during the ground shaking. The maximum curvature among all piers, $\phi_{\max}$, was then selected as the EDP. The curvature direction was the transversal, since in the records were applied only in the that direction. The collapse limit was assumed to be when the first pier reached 60 mrad of base curvature, since as seen in Figure 3 there is almost no moment resisting capacity in the pier at that level of deformation. Other failure mechanisms, such as pier shear failure, deck unseating, and foundation or abutment failure, could also be considered in more detailed studies. For instance, Borzi et al. [20] highlighted these mechanisms for older Italian bridges, where shear failure and deck unseating were observed in past seismic events, and the two limit states were subsequently incorporated into a global demand-capacity envelope EDP, as described by Jalayer et al. [21].

4 HAZARD ANALYSIS

PSHA was carried out for a site in Erzincan, Turkey using the OpenQuake [22] open-source software for seismic hazard and risk assessment developed by the Global Earthquake Model Foundation. The input source model was the ESHM20 model [23] and the ground motion model (GMM) was the one proposed by Aristeidou et al. [5]. Erzincan was selected as the case study site as it exhibits one of the highest seismic activities in Europe and Middle East. This high seismicity facilitates the characterisation of the bridges' performance throughout the whole range of nonlinear response without needing to reach very high return periods.

The hazard curves of each conditioning IM used to analyse the 1st bridge are shown in Figure 4. The hazard curves of the IMs at other periods are omitted here for brevity. Additionally, the hazard disaggregation for $FIV3$ at the fundamental period of bridge 1 is given in Figure 5. The

rest of the disaggregation plots are omitted here for brevity. It can be seen that most of the hazard is controlled by source-to-site distances below 30 km and magnitude mostly above 6.5. There are many scenarios, rup, contributing to the hazard, especially in low return periods, but for simplicity only the modal rupture scenario was used to select ground motions at each return period as a first-order representation of the full disaggregation distribution.

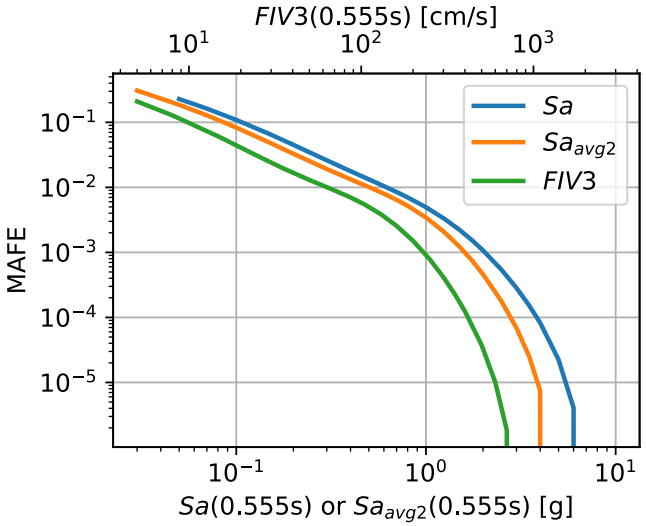

Figure 4: Hazard curves of IM* of bridge 1

It is also important to have a sense of the dispersions of IM$|rup$ for the different conditioning IMs used in this study. In this case, the input rupture parameters used in the estimation of logarithmic standard deviation, $\sigma_{\mathrm{IM}|\mathrm{rup}}$, are irrelevant, because the GGMM used is homoscedastic (i.e., dispersion of IMs is independent of rupture parameters). Therefore, the $\sigma_{\mathrm{IM}|\mathrm{rup}}$ calculated for a period of 0.5 s (which is an intermediate period between the T_1 of the analysed structures) was 0.66, 0.58, and 0.58 for Sa, average spectral acceleration, Sa_{avg2}, and $FIV3$, respectively. The lower GGMM dispersion of $FIV3$ and Sa_{avg2} indicates a better predictability with respect to other IMs and further encourages their usage in risk analyses. It should be noted here that Sa_{avg2} refers to a period range from $0.2T$ to $2T$, and Sa_{avg3} to a period range from $0.2T$ to $3T$.

5 GROUND MOTION SELECTION SCHEMES: CONDITIONING IMS, MATCHED SPECTRA AND MATCHED IMS

The GCIM ground motion selection approach, introduced by Bradley [13] extends the principles of the CS approach [12] by allowing the matching IMs to differ from the conditioning IM. This addresses a key limitation of the CS approach, which focuses on spectral accelerations while neglecting other characteristics of ground motions which may or may not be pertinent to the structural system studied. It is well-established that the severity of a ground motion in non-linear systems depends not only on its spectral accelerations but also on its velocity pulses, duration, and energy. Sa, by definition, represents the peak response of an elastic single-degree-of-freedom (SDOF) oscillator at a specific period and therefore fails to account for other important ground motion features.

The CS approach is based on the assumption that spectral accelerations follow a multivariate lognormal distribution. Building on this, the GCIM approach generalises this concept by proposing that any arbitrary vector of IMs, for a given seismic scenario, follows a multivariate

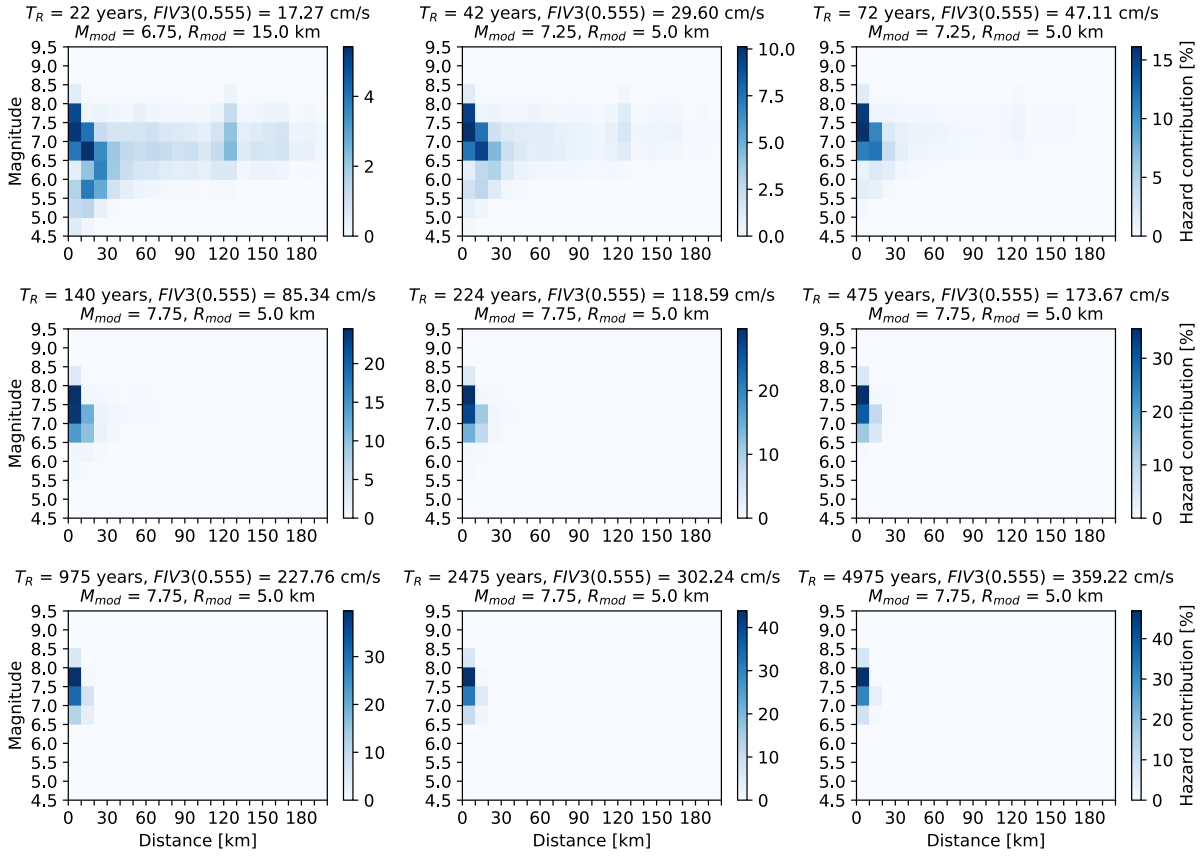

Figure 5: Hazard disaggregation of $FIV3$ at 0.555 s for the nine return periods investigated

lognormal distribution. This vector can include any scalar IMs, making the GCIM approach more versatile. Regarding the validity of this assumption, it is widely recognised that most IMs exhibit marginal lognormal distributions, as supported by regression analyses on $\ln(\mathrm{IM})$ in empirical GMMs. The conditional mean and standard deviation of the included IMs are therefore expressed in Equations 1 and 2.

$$\mu_{\ln \mathrm{IM_i}|\ln \mathrm{IM^*},\mathrm{rup}} = \mu_{\ln \mathrm{IM_i}|\mathrm{rup}} + \sigma_{\ln \mathrm{IM_i}|\mathrm{rup}} \cdot \rho_{\ln \mathrm{IM}_i,\ln \mathrm{IM^*}} \cdot \epsilon_{\ln \mathrm{IM^*}} \tag{1}$$

$$\sigma_{\ln \mathrm{IM_i}|\ln \mathrm{IM^*},\mathrm{rup}} = \sigma_{\ln \mathrm{IM_i}|\mathrm{rup}} \cdot \sqrt{1 - \rho^2_{\ln \mathrm{IM_i},\ln \mathrm{IM^*}}} \tag{2}$$

where, $\mathrm{IM_i}$ is the matched IMs, IM* is the conditioning IM, μ is the target mean, σ is the target standard deviation, ρ the cross-correlation coefficient, and ϵ the normalised residual [24].

In the ground motion selection schemes investigated here, three different conditioning IMs (IM*) were included, namely $Sa(T_1)$, $Sa_{\mathrm{avg2}}(T_1)$, and $FIV3(T_1)$. Also, a combination of several IMs, for which the theoretical distribution was also conditionally matched ($\mathrm{IM_i}$), namely $Sa(T)$, Ds_{575}, $Sa_{\mathrm{avg3}}(T)$, $FIV3(T)$, and $Sa_{\mathrm{avg2}}(T)$, were included. All the different ground motion record selection cases along with their conditioning and matched IMs are listed in Table 2. For the period-dependent IMs, where 'T' is denoted it means that the whole spectrum at a range of periods was matched, and 'T_1' means that the IM at the first period of each structure was matched.

No rupture parameter limits were applied in the selection of ground motions, but a maximum scale factor of 8 was set. Both horizontal components of the pool of recorded motions

Table 2: Ground motion input cases

Case No.	IM*	IM_i			
0	$Sa(T_1)$	—	—	—	—
1	$Sa(T_1)$	$Sa(T)$	—	—	—
2	$Sa(T_1)$	$Sa(T)$	Ds_{575}	$Sa_{\text{avg3}}(T_1)$	$FIV3(T_1)$
3	$Sa(T_1)$	$Sa(T)$	—	$Sa_{\text{avg3}}(T_1)$	$FIV3(T_1)$
4	$Sa(T_1)$	$Sa(T)$	Ds_{575}	—	—
5	$Sa_{\text{avg2}}(T_1)$	$Sa(T)$	—	—	—
6	$FIV3(T_1)$	$Sa(T)$	—	—	—
7	$Sa_{\text{avg2}}(T_1)$	—	—	$Sa_{\text{avg2}}(T)$	—
8	$FIV3(T_1)$	—	—	—	$FIV3(T)$
9	$Sa_{\text{avg2}}(T_1)$	—	Ds_{575}	$Sa_{\text{avg2}}(T)$	—
10	$FIV3(T_1)$	—	Ds_{575}	—	$FIV3(T)$

were included in the selection pool, in other words the amount of possible ground motions to be used for the analysis were double the amount of available recordings. This is done because the bridge is excited unidirectionally. However, in the hazard calculations and in generating the target IM distributions, the *RotD50* or the geometric mean horizontal component definitions were used. It should be noted that the ideal scenario would be to use the arbitrary horizontal component definition for hazard and ground motion selection targets. Nevertheless, the difference is expected to be small and would not affect the relative conclusions drawn in this study. A set of 50 records were selected for each stripe. As an example, the target and selected spectra and cumulative distribution functions (CDFs) of selection Case 2 for the structure B-1 at 475 year return period are illustrated in Figures 6, 7, and 8. This case is chosen to be presented here as it has the most IM_i. It is clear how the selected records match the target distributions very well, for all IM types explored.

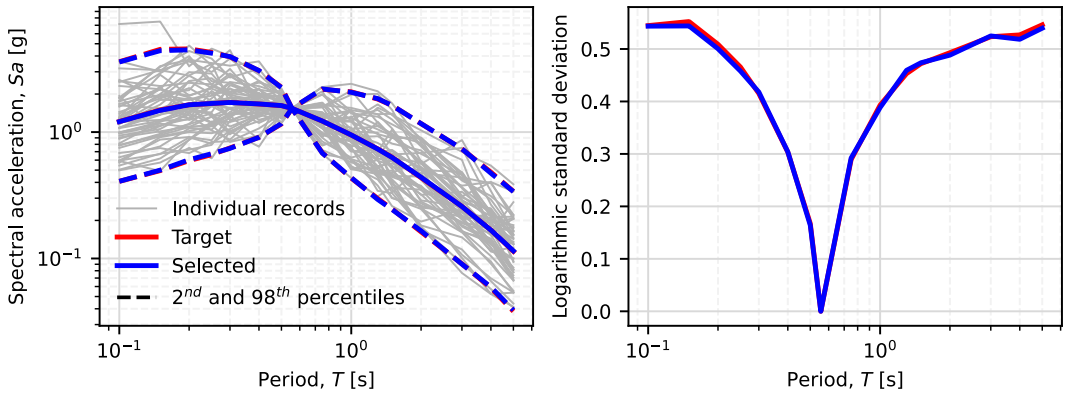

Figure 6: Sa spectrum and comparison of the target and selected dispersions for record selection Case 2 of bridge B-1 at 475 years return period

6 RESULTS

6.1 MSA results

With the ground motion record sets identified in Section 5 for each selection case, return period, and bridge structure, MSA was carried on the numerical model of each bridge structure.

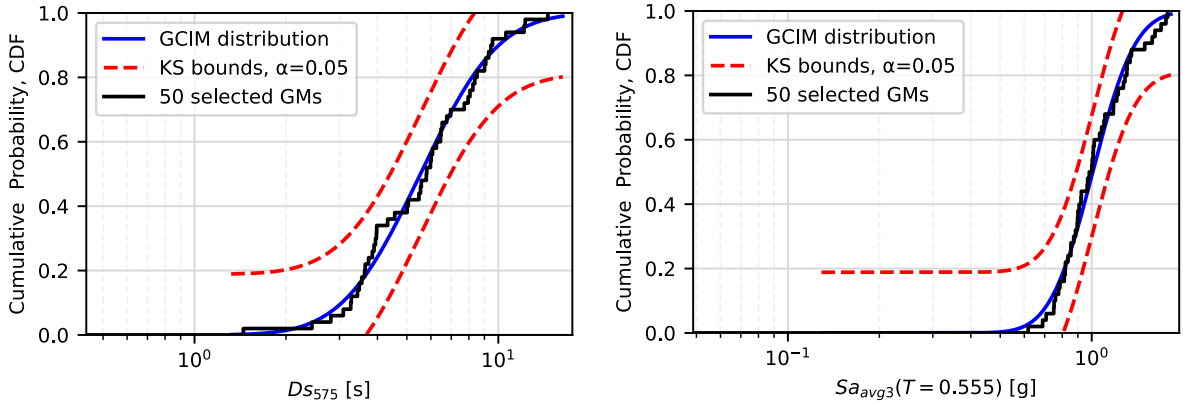

Figure 7: Ds_{575} (left) and Sa_{avg3} (right) theoretical and empirical CDF for record selection Case 2 of bridge B-1 at 475 years return period

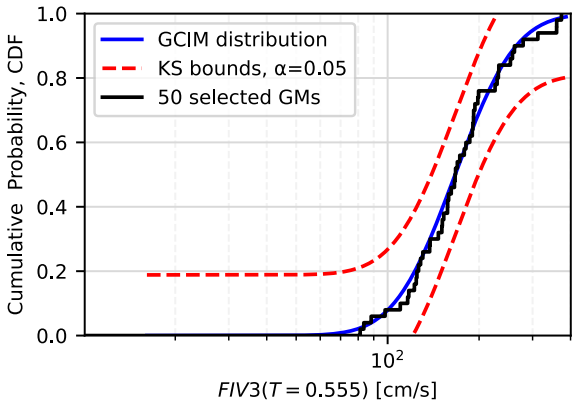

Figure 8: $FIV3$ theoretical and empirical CDF for record selection Case 2 of bridge B-1 at 475 years return period

The output of this analysis is an empirical distribution of bridge response, characterised via an EDP (in this case $\phi_{\max}$), versus an IM level corresponding to a specific return period. As an example, the MSA results for the case study bridge B-1 and ground motion selection Case 5 are illustrated in Figure 9. Each scatter point represents an individual response ordinate from a ground motion record scaled to a specific intensity stripe, which amount to a total of 9 intensity levels. The response ordinates of only the non-collapse cases are shown in the plot, for which the logarithmic mean and ± 1 standard deviation are also illustrated. Also shown in the right-hand side of the figure is the probability of collapse in each intensity level. The logarithmic mean of non-collapse response values, along with the denoted probability of collapse, indicate the increase in bridge demand with increasing shaking intensity. It can be also observed from Figure 9 the increased standard deviation of EDP response with increasing IM level, but it should be noted that the axes are not logarithmic.

6.2 Intensity-based evaluation

One of the points of comparison can firstly be the dispersion in demand for a given intensity, $\beta_{\text{EDP|IM}}$, which can help in gaining insights into the predictive capability of each ground motion input case. Another point can be the median demand for a given intensity, $\eta_{\text{EDP|IM}}$, which is also reported in this section and discussed, since it is important to investigate the im-

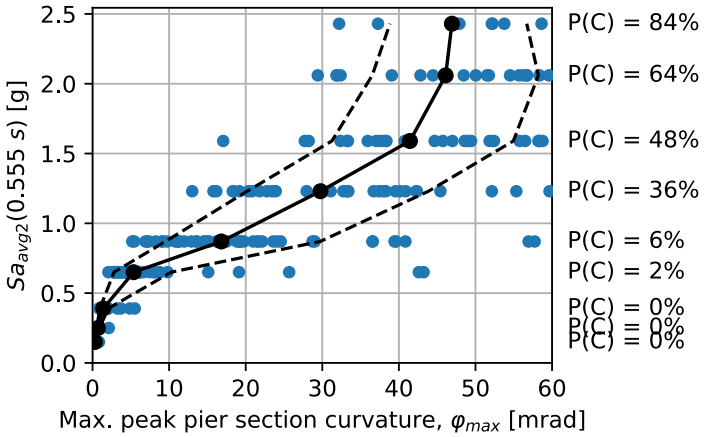

Figure 9: MSA results obtained with the ground motion input 5 on case study bridge B-1. Also depicted is the logarithmic mean and ± 1 standard deviation of the non-collapse cases, and the probability of collapse resulting from each intensity level

pact of employing ground motions with different characteristics in each case on the structural response. Although demand-based evaluations are more relevant for risk assessment purposes, intensity-based evaluations remain commonly prescribed in design codes [25, 26]. Furthermore, intensity-based evaluations serve as the foundation for the structural analysis inputs required in loss estimation, as exemplified by Mackie et al. [27].

Figure 10 depicts the $\eta_{\mathrm{EDP|IM,NC}}$ for all the bridge structures and all the ground motion input cases as a function of return period. It should be mentioned that the median is conditioned on no collapse. In the legend of the plot, the code name for each case is also given. The first IM is the conditioning one, while the IMs after the dash symbol are the ones whose theoretical GCIM distribution is been matched by the record selection. The ones denoted with "(T)" are the ones whose spectrum is matched, whereas the other period-dependent IMs without "(T)", were matched only at the 1st period of each structure. Bridge 4 presents the lowest EDP medians, and therefore has the lowest vulnerability and also the lowest probability of collapse in each return period. This is because of the regular distribution of pier heights along the length of the bridge, the same with B-3 and B-5. The most obvious observation in Figure 10 is Case 0, which gives the lowest response medians. This is simply because the selected mean spectrum of the selected ground motions is notably lower than the target mean spectrum for the site, since the Sa spectrum was not matched although the conditional variability is slightly higher and not matching the target distribution either. The target and selected spectra for this case are omitted here for brevity. In addition to that, the duration of records obtained in Case 0 is shorter that the one obtained in Case 1 which further decreases the severity of the selected ground motion on degrading systems [28]. Another point that stands out is the higher $\eta_{\mathrm{EDP|IM}}$ obtained in regular bridges with the cases that have $FIV3$ as the conditioning IM.

Furthermore, it should be noted in Figure 10 that Cases 2 and 3 present lower EDP medians than case 1. This is mostly because Case 1 includes records with higher-than-expected durations, whereas Cases 2 and 3 match the duration distribution expected at the site. This is where the majority of the difference comes form, since the distribution of other IMs is very similar in these cases.

Figure 11 presents the $\beta_{\mathrm{EDP|IM,NC}}$ as a function of return period for all the bridges and ground motion input cases. It can be seen that the general trend of this dispersion is that it starts from a low dispersion in low return periods, T_{R}, gets higher in the intermediate T_{R} and then lower

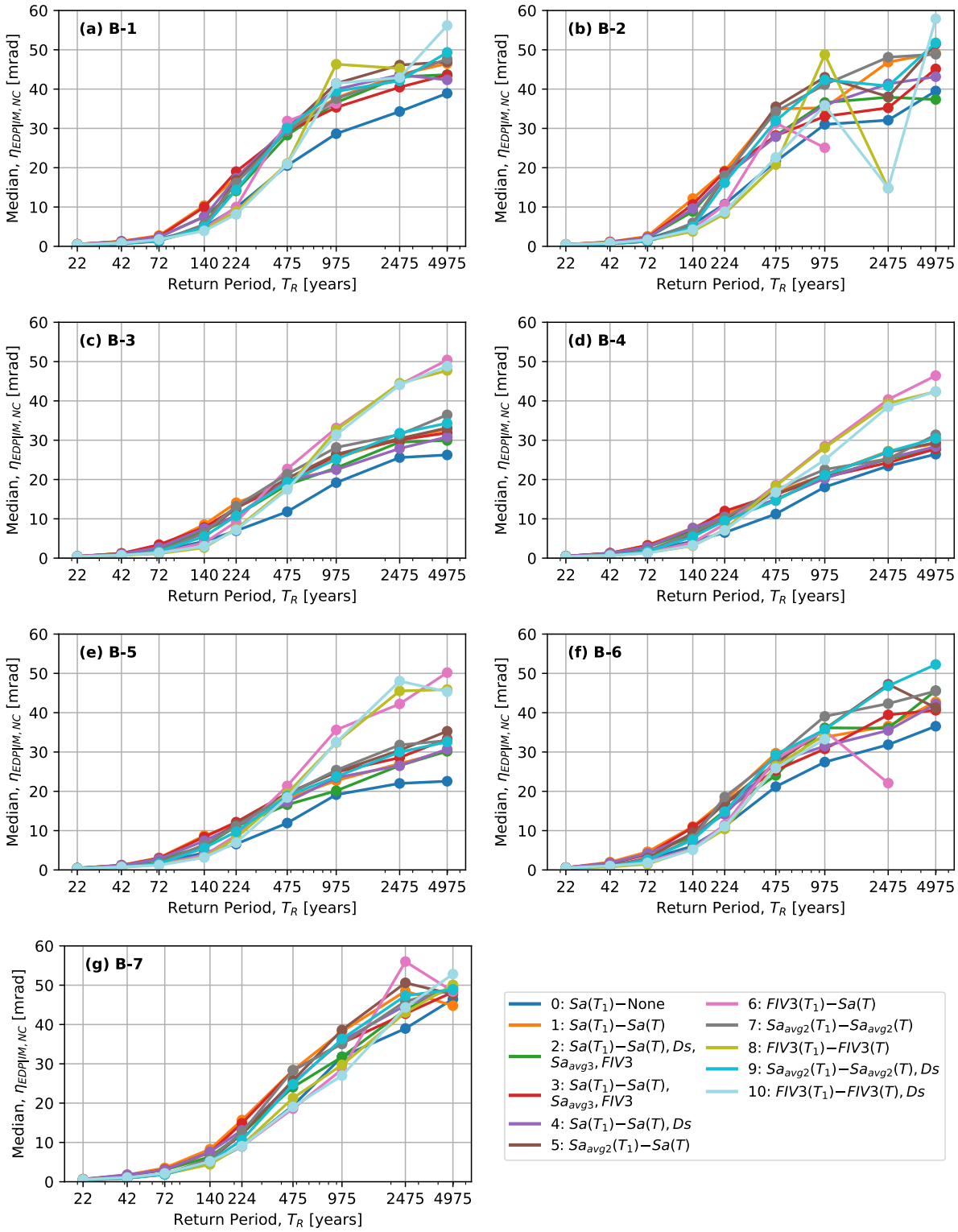

Figure 10: Median of EDP given IM level given no collapse

in high T_{R}. The reason for having lower dispersion in higher return periods is because many records cause collapse in the case study structures, since for the scope of this exercise are located in high seismicity area, and additionally degradation is added in the numerical models. The more severe records cause collapse, and therefore excluded from the dispersion calculation, since it is conditioned on no collapse, which results in lower $\beta_{\mathrm{EDP|IM,NC}}$.

It can be observed that for most return periods, Case 9 (i.e., Sa_{avg2} GCIM with matching Ds_{575}) exhibits the lowest $\beta_{\mathrm{EDP|IM,NC}}$. Meanwhile, in regular bridges (i.e., B-3, B-4, and B-5), Cases 6, 8, and 10 (i.e., the ones with $FIV3$ as the conditioning IM) are the most efficient ones for return periods of 475 years and above, which corroborates past observations for these IMs [16, 29, 30, 31].

7 IMPLICATIONS FOR BRIDGE DAMAGE MECHANISMS AND RISK ASSESSMENT

The findings presented in this study have direct implications for understanding bridge damage mechanisms and advancing risk assessment methodologies. The analysis of different ground motion selection strategies highlights the role of spectral shape, cumulative energy demand, and duration effects in influencing bridge response, all of which are critical for predicting damage evolution. This is especially the case for bridges that experience strength and stiffness degradation during their lifetime and during the seismic excitation.

Through the use of Sa, Sa_{avg}, $FIV3$, and Ds_{575}, this study captures aspects of ground motion that correlate with progressive stiffness degradation, plastic hinging, and strength loss in bridge piers. The ϕ_{max} used as the EDP effectively represents inelastic deformations in bridge piers, which is a commonly observed failure mechanism in past earthquakes.

Moreover, the comparative analysis of different ground motion selection strategies reveals how conditioning on Sa_{avg} and $FIV3$ leads to reduced response dispersion, thereby more accurate structural response estimates. This insight is crucial for enhancing regional risk assessments, where having more control over the record-to-record variability can lead to more reliable infrastructure resilience planning.

In alignment with broader efforts to systematically characterise bridge damage mechanisms, this work also provides a foundation for integrating advanced IMs into post-earthquake damage assessment frameworks. Future extensions could incorporate pier shear failure, bearing damage, foundation settlement, and multi-support excitation effects, ensuring a more comprehensive representation of bridge seismic vulnerabilities.

8 SUMMARY AND CONCLUSIONS

A comprehensive analysis was conducted to evaluate the impact of next-generation intensity measures (IMs) on the seismic risk assessment of bridge structures. Recently developed generalised ground motion model (GGMM) and correlation models were employed to facilitate the selection of ground motions using advanced approaches, such as the generalised conditional intensity measure (GCIM) method. This approach ensures that key features of ground motions beyond spectral acceleration, such as spectral shape, duration and velocity, are appropriately represented and matched during selection.

A suite of multi-span bridge structures with varying pier heights and span configurations was analysed using numerical models built in OpenSeesPy. Ground motion records were selected and scaled according to different strategies, including just scaling to the conditioning IM, conditional spectrum (CS)-based, and GCIM-based selection. The multiple stripe analysis (MSA)

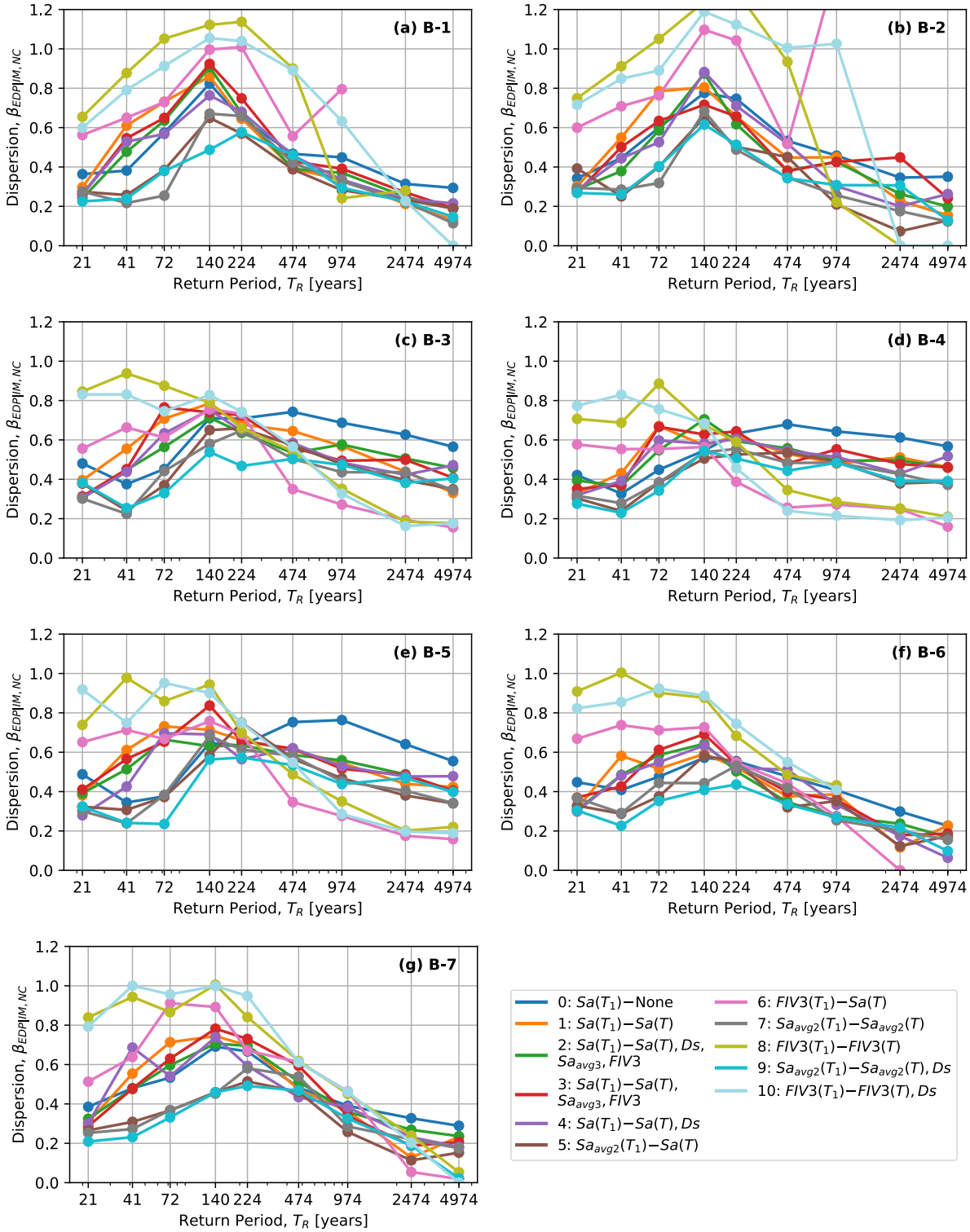

Figure 11: Dispersion of EDP given IM level given no collapse

method was used to quantify structural demands at each intensity level.

The conclusions regarding the comparisons between the different ground motion selection cases are outlined as follows:

- Cases 0 and 1: Impact of just scaling the ground motions to spectral acceleration at the 1st period of vibration, $Sa(T_1)$, in comparison to also matching the Sa spectrum (i.e., conditional spectrum). Case 0 gave lower structural response for the same IM level, because of the lower-than-expected Sa spectrum of the selected ground motions. The impacts of this were also evident in the dispersions, which highlighted the importance of matching the target distribution of the Sa spectrum, and not just the conditioning one.

- Cases 1 and 2: Comparison between conditional spectrum of Sa and GCIM. The CS approach gave ground motions with higher-than-expected significant duration, Ds_{575}, which resulted in higher EDP medians. The dispersions were somewhat lower in Case 2, and therefore presented higher efficiency. Nevertheless, the differences in dispersion were small.

- Cases 1, 2, 3, and 4: They are included to check whether the differences between Cases 1 and 2 come mainly from the duration. In fact, Cases 2 and 4 give similar results, while Cases 1 and 3 also exhibit similar results between them. Therefore we can conclude that the differences between Cases 1 and 2 come primarily from matching the Ds_{575}.

- Cases 1, 5, and 6: Comparison of the different conditioning IMs (i.e., Sa, average spectral acceleration, Sa_{avg2}, and filtered incremental velocity, $FIV3$, respectively) while matching the Sa spectrum. Case 1 resulted in low dispersion only in lower return periods, and then the dispersion quickly rises in the intermediate return periods. Case 5 was more efficient in the irregular bridges, while Case 6 dominated with regards to efficiency in most of the return periods of the regular bridges.

- Cases 5 and 7: This is to investigate the difference between conditioning on Sa_{avg2} and matching the Sa spectrum, with the CS of Sa_{avg2}. Dispersions and medians were very similar between the two cases. This suggests that one can select any of the two schemes and obtain very similar results.

- Cases 6 and 8: This is to investigate the difference between conditioning on $FIV3$ and matching the Sa spectrum, with the CS of $FIV3$. Dispersions, medians and risk estimates are very similar between the two cases, with Case 6 resulting in slightly lower dispersions.

- Cases 9 and 10, versus the all rest: The GCIM method of conditioning on Sa_{avg2} and $FIV3$, respectively, while matching their corresponding spectrums and the Ds_{575} theoretical distribution at the site, seem to be best cases. Case 9 is better for the initial and intermediate stages of nonlinearity, while Case 10 is better for the deeper stages of nonlinear response and near collapse. Furthermore, Case 9 exhibits better results in irregular bridges, while Case 10 in regular bridges.

This work demonstrated the practical benefits of next-generation IMs, such as $FIV3$ and Sa_{avg}, in improving both the accuracy and consistency of seismic demand estimations. Specifically, the GCIM-based approach proved highly effective in reducing the dispersions and providing more accurate median estimates of structural response, while ensuring hazard consistency—a critical factor often overlooked in traditional selection methods. The findings further

highlighted the sensitivity of IM efficiency to structural regularity, with velocity-based IMs like $FIV3$ excelling for regular bridges and Sa_{avg2} exhibiting superior performance for irregular structures.

Overall, this work bridges the gap between state-of-the-art ground motion selection techniques and practical applications, offering a robust and hazard-consistent framework for fragility analysis and risk estimation. The comparisons and conclusions drawn here can serve as a foundation for future research and considerations in performance-based design and bridge vulnerability assessment, ensuring greater resilience of critical infrastructure under seismic loading.

ACKNOWLEDGEMENTS

This work was developed under the financial support of the Italian Department of Civil Protection, within the ReLUIS 2024-2026 WP Calvi research project, which is gratefully acknowledged. The authors would also like to thank the Djura company for providing their record selection tool.

REFERENCES

[1] N. Luco and C. A. Cornell, "Structure-specific scalar intensity measures for near-source and ordinary earthquake ground motions," *Earthquake Spectra*, vol. 23, no. 2, pp. 357–392, 2007.

[2] Q. Huang, P. Gardoni, and S. Hurlebaus, "Probabilistic Seismic Demand Models and Fragility Estimates for Reinforced Concrete Highway Bridges with One Single-Column Bent," *Journal of Engineering Mechanics*, vol. 136, no. 11, pp. 1340–1353, 2010.

[3] M. Kohrangi, D. Vamvatsikos, and P. Bazzurro, "Pulse-like versus non-pulse-like ground motion records: Spectral shape comparisons and record selection strategies," *Earthquake Engineering & Structural Dynamics*, vol. 48, no. 1, pp. 46–64, 2019.

[4] H. Dávalos and E. Miranda, "Evaluation of FIV3 as an Intensity Measure for Collapse Estimation of Moment-Resisting Frame Buildings," *Journal of Structural Engineering*, vol. 146, no. 10, pp. 1–14, 2020.

[5] S. Aristeidou, D. Shahnazaryan, and G. J. O'Reilly, "Artificial neural network-based ground motion model for next-generation seismic intensity measures," *Soil Dynamics and Earthquake Engineering*, vol. 184, p. 108 851, 2024.

[6] S. Aristeidou, D. Shahnazaryan, and G. J. O'Reilly, "Correlation Models for Next-Generation Amplitude and Cumulative Intensity Measures using Artificial Neural Networks," *Earthquake Spectra*, vol. 41, no. 1, pp. 851–875, 2025.

[7] HAZUS, "Multi-hazard loss estimation methodology - earthquake model," FEMA-National Institute of Building Sciences, Washington, DC, USA, 2003.

[8] M. Villar-Vega et al., "Development of a Fragility Model for the Residential Building Stock in South America," *Earthquake Spectra*, vol. 33, no. 2, pp. 581–604, 2017.

[9] C. Del Gaudio et al., "Empirical fragility curves from damage data on RC buildings after the 2009 L'Aquila earthquake," *Bulletin of Earthquake Engineering*, vol. 15, no. 4, pp. 1425–1450, 2017.

[10] CEN, *Eurocode 8: Design of Structures for Earthquake Resistance - Part 2: Bridges (EN 1998–2:2005)*, 2005, Brussels, Belgium.

[11] ASCE, *Minimum design loads for buildings and other structures*, ASCE 7-16. American Society of Civil Engineers, 2017, pp. 1–889, Reston, VI.

[12] J. W. Baker, "Conditional Mean Spectrum: Tool for Ground-Motion Selection," *Journal of Structural Engineering*, vol. 137, no. 3, pp. 322–331, 2011.

[13] B. A. Bradley, "A generalized conditional intensity measure approach and holistic ground-motion selection," *Earthquake Engineering & Structural Dynamics*, vol. 39, no. 12, pp. 1321–1342, 2010.

[14] K. Tarbali and B. A. Bradley, "Ground motion selection for scenario ruptures using the generalised conditional intensity measure (GCIM) method," *Earthquake Engineering & Structural Dynamics*, vol. 44, no. 10, pp. 1601–1621, 2015.

[15] R. Pinho, R. Monteiro, C. Casarotti, and R. Delgado, "Assessment of continuous span bridges through nonlinear static procedures," *Earthquake Spectra*, vol. 25, no. 1, pp. 143–159, 2009.

[16] G. J. O'Reilly, "Seismic intensity measures for risk assessment of bridges," *Bulletin of Earthquake Engineering*, vol. 19, no. 9, pp. 3671–3699, 2021.

[17] M. Zhu, F. McKenna, and M. H. Scott, "OpenSeesPy: Python library for the OpenSees finite element framework," *SoftwareX*, vol. 7, pp. 6–11, 2018.

[18] G. J. O'Reilly and R. Monteiro, "On the efficient risk assessment of bridge structures," *COMPDYN 2019 - 7th international conference on computational methods in structural dynamics and earthquake engineering*, 2019, pp. 473–483, Crete Island, Greece.

[19] M. J. N. Priestley, F. Seible, and G. M. Calvi, *Seismic design and retrofit of bridges*. New York: John Wiley & Sons, 1996, p. 686.

[20] B. Borzi, P. Ceresa, P. Franchin, F. Noto, G. M. Calvi, and P. E. Pinto, "Seismic Vulnerability of the Italian Roadway Bridge Stock," *Earthquake Spectra*, vol. 31, no. 4, pp. 2137–2161, 2015.

[21] F. Jalayer, P. Franchin, and P. E. Pinto, "A scalar damage measure for seismic reliability analysis of RC frames," *Earthquake Engineering & Structural Dynamics*, vol. 36, no. 13, pp. 2059–2079, 2007.

[22] GEM, "The OpenQuake-engine User Manual," *Global Earthquake Model (GEM) OpenQuake Manual for Engine version 3.18.0*, 2022.

[23] L. Danciu et al., "The 2020 update of the European Seismic Hazard Model: Model Overview," Tech. Rep. EFEHR Technical Report 001, v1.0.0, 2021.

[24] J. W. Baker and C. A. Cornell, "Spectral shape, epsilon and record selection," *Earthquake Engineering & Structural Dynamics*, vol. 35, no. 9, pp. 1077–1095, 2006.

[25] T. Lin, C. B. Haselton, and J. W. Baker, "Conditional spectrum-based ground motion selection. Part II: Intensity-based assessments and evaluation of alternative target spectra," *Earthquake Engineering & Structural Dynamics*, vol. 42, no. 12, pp. 1867–1884, 2013.

[26] J. Poveda and G. J. O'Reilly, "Influence of Ground Motion Record Selection on Higher Modes: A Comparison of UHS and CS Approaches," *Third Croatian Conference on Earthquake Engineering (3CroCEE)*, 2025, Split, Croatia.

[27] K. R. Mackie, J.-M. Wong, and B. Stojadinović, "Post-earthquake bridge repair cost and repair time estimation methodology," *Earthquake Engineering & Structural Dynamics*, vol. 39, no. 3, pp. 281–301, 2010.

[28] R. Chandramohan, J. W. Baker, and G. G. Deierlein, "Quantifying the influence of ground motion duration on structural collapse capacity using spectrally equivalent records," *Earthquake Spectra*, vol. 32, no. 2, pp. 927–950, 2016.

[29] H. Dávalos and E. Miranda, "Filtered incremental velocity: A novel approach in intensity measures for seismic collapse estimation," *Earthquake Engineering & Structural Dynamics*, vol. 48, no. 12, pp. 1384–1405, 2019.

[30] S. Aristeidou and G. J. O'Reilly, "Exploring the Use of Orientation-Independent Inelastic Spectral Displacements in the Seismic Assessment of Bridges," *Journal of Earthquake Engineering*, vol. 28, no. 12, pp. 3515–3538, 2024.

[31] A. K. Kazantzi and D. Vamvatsikos, "Intensity measure selection for vulnerability studies of building classes," *Earthquake Engineering & Structural Dynamics*, vol. 44, no. 15, pp. 2677–2694, 2015.